



The 4D Reconstruction of Dynamic Geologic Processes for Renowned Geologic Features

Jiateng Guo^{1*}, Zhibin Liu¹, Xulei Wang¹, Lixin Wu², Shanjun Liu¹, Yunqiang Li¹

¹School of Resources and Civil Engineering, Northeastern University, NO. 3-11, Wenhua Road, Heping District, Shenyang, 110819, China;

²School of Geosciences and Info-Physics, Central South University, Lushan Nanlu 932, Yuelu District, Changsha 410012, China.

Correspondence to: Jiateng Guo (guojiateng@mail.neu.edu.cn; Tel.: +86-24-8368-7693)

Abstract. The three-dimensional (3D) visualization of geological structures and the dynamic simulation of geologic evolutionary processes are helpful when studying the formation of renowned geologic features. However, most of the existing 3D modelling software is based on raster models, which is unable to generate smooth geologic boundaries. This work proposes a three-dimensional and temporally dynamic (i.e., 4D) modelling method using parametric functions and vector data structures, which can dynamically build geologic evolutionary vector models of well-known geologic features. First, we extract the typical features of different kinds of geologic formations and represent them using different parameters. Next, appropriate parametric functions are selected to simulate these geologic formations according to the characteristics of the individual structures. Then, we designed and developed a 4D vector modelling software to simulate the geologic evolution of these features. Finally, we simulated an area with complex geologic structures and selected six real-world geologic features, such as the Piqiang Fault in China and the Eye of the Sahara in the Sahara Desert, as case studies. The modelling results show that a regional geologic evolutionary model that contains smooth boundaries can be established quickly using this method. This work will support studies into the formation of these renowned geological features and make the representation of geologic processes more intuitive.

1 Introduction

Geological relics are features on the surface of the Earth that manifested at some point during the Earth's geologic history. The analysis of regional geological evolutionary processes is central to the study of how geological relics formed. Regional geological evolution refers to the process of continuous change and transformation of a geological body due to the action of certain regional forces (be they external, internal, or artificial). Eventually, these forces alter the composition and structure of the local stratigraphic units and can change the surface morphology. Understanding the evolutionary processes that impact geological formations is critical to the study of geological evolution, because not only do these processes control the formation and evolution of fractures but also determine the spreading and superposition of other geologic structures. The analysis of



geological evolutionary processes also plays a crucial role in determining structural morphology, assessing bioaccumulation, assessing coalbed gas and the abundance of mineral resources (Favre et al., 2015; Li et al., 2021; Rahbek et al., 2019; Zhai et al., 2013; Zhou et al., 2022). Therefore, studying the geological and structural evolution of a region and simulating it can help people better understand how the geology of the region developed.

35 The traditional method of studying geological evolutionary processes is to analyse the data directly and then visualize the results obtained from the analysis in the form of geologic cross sections and profiles (Bozzano et al., 2008; Van Hinsbergen et al., 2020). Some **scholars** also use static 3D models for these visualizations. A common method of interpretation involves using the survey data to develop a geological model for a specific moment in time and then extracting cross-sections along arbitrary directions within the 3D model (Abdullah et al., 2022; Adelu et al., 2019), which makes the interpretation process much easier. 40 Essentially, the evolutionary process is still represented within the cross-section. However, subsurface geological phenomena are 3D by nature, and two-dimensional (2D) profiles cannot clearly express the complete evolution of the subsurface. These specialized 2D depictions of the evolutionary processes are not sufficient visual representations of the geologist's ideas and knowledge. They are only convenient for discussing and disseminating knowledge among peers and experts (Lidal et al., 2012). **These products remain inaccessible to general audiences and make communicating ideas challenging.** This is a problem since 45 geologists prefer to be able to communicate their results in a way that can be understood by nonexperts and decision makers alike.

Therefore, the numerical simulations are also applied to geological evolutionary studies. This involves conducting simulation experiments for each phase of structural movement and adjusting the simulation parameters as the experiments progress; finally, the actual evolutionary processes operating within the modelled domain are obtained (Chen et al., 2010; Wu et al., 2022). There are also scholars who use existing software such as Adobe to manually draw and animate the geological evolution process to facilitate communication (Geology-an Introduction, 2012). However, these methods present their own challenges. **They are time consuming, and because of a lack of generality between individual models, the researcher may be required to start over for different geological regions, which leads to highly repetitive workflows.**

Natali et al. (2012) proposed a method for synthesizing 3D models from 2D sketches. Based on this, Lidal et al. (2013) 55 proposed a sketch based approach to reconstruct geological evolutionary processes, which **all** for the model process model to be visualized and **for the reasoning behind it to be more clearly conveyed.** This approach can quickly construct a 3D geological evolutionary model from hand sketches. However, the final model obtained by this method only adds a depth to the 2D image, and the structure along the depth direction cannot be simulated. Jessell et al. (1996; 2022) proposed an integrated orthorectification technique for simulating the geophysical response of 3D structures and geologic bodies that have undergone 60 multiple stages of deformation. This method can simulate the deformation history of a region by including a series of historical events and the model can then obtain the corresponding geological data. Cockett et al. (2016) created a learning tool, Visible Geology, capable of exploring the evolutionary processes of different geological body in one-dimensional (1D), 2D, and 3D space. However, these techniques all have some drawbacks; for example, the method used to simulate geological structures **is too simple**, the generated folds can only run through the whole model, the intrusive rocks are represented as a simple layer of



65 vertical strata, and the models are all raster models, which cannot smoothly depict geological boundaries (Zhu et al., 2022).
Therefore, there has been a lack of a 4D vector modelling method for the simulation of geological evolutionary processes. This
method includes more modules available for feature construction and can quickly reconstruct dynamic geological evolutionary
processes, which can then be communicated to a general audience.

Geological evolutionary processes are generally inferred by geological experts based on scattered data and their own
70 knowledge. **Therefore, the complete process clearly exists only in the minds of geological experts and, confined to two-
dimensional pencil and paper drawings, the process cannot be clearly represented.** It will not only take a lot of time to model
each process, but the geological data for each process cannot be obtained to support this endeavour. Here we propose a method
to quickly construct a model that simulates geologic evolutionary processes according to the need for the these process to be
visually expressed. First, this model is generalized and parameterized for various complex geological formations that may
75 have occurred during geological evolutionary. Then, different parameter functions are used to simulate the different kinds of
geological formations. Second, each kind of geological structure is modularized, and a tetrahedron field is used to organize the
whole model so that it can easily incorporate a geological structure module to the current model. This method can model
geological evolution quickly and dynamically based on our software. Finally, the key operations of changing geological
morphology are stored for each step of the geological timeline, which can easily replicate the entire evolution process.
80 Additionally, each operation in the history timeline is exported for subsequent reproduction and modification. Using this
technique, geologists can quickly construct a simplified history of geotectonic motion for a region based on the geological
information considered (such as the evolution of the regional geology).

In this study, we modularized five geological structures, including tilt, fold, fault, simple unconformity, and intrusive
rocks, which can be superimposed in any order. This article is structured as follows: Chapter 2 presents the rationale for the
85 generalization of each geologic formation, Chapter 3 describes the simulation methods used for each formation, Chapter 4
performs a typical case simulation, Chapter 5 discusses recommendations for future research, and Chapter 6 presents the
conclusion.

2 Principle of constructive parameterization

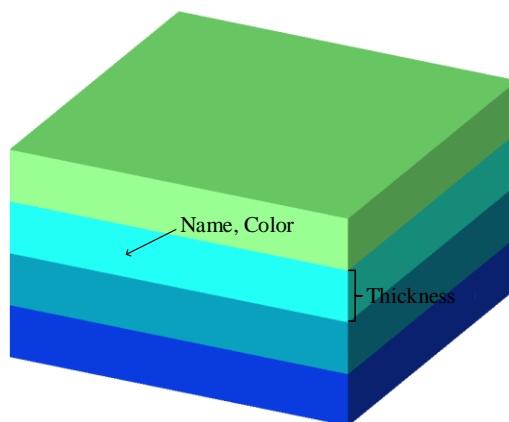
First, this study generalizes some basic geological formations, and different kinds of geological structures are parameterized
90 according to the basic elements of geological formations. This enables the model to differentiate geological structures and to
separate them into different modules, thus ensuring that a diversity of geological structures is expressed within the model so
as to better simulate the diverse forms of geological structures found in nature.

2.1 Stratigraphic data

A stratum is a layer or group of rock layers that has some uniform characteristics and properties and is clearly distinguishable
95 from the units above and below. In this study, we simulate the simplest sedimentary stratum by reducing sedimentary strata



that may have some variable thickness to a uniform thickness. **Therefore, a stratum can be described by the following three parameters** (Fig. 1): (1) *Name*, which denotes the name of the stratum; (2) *Colour*, which indicates the colour used to represent the stratum and is also used to represent a certain or certain group of stratum characteristics; (3) *Thickness*, which refers to the thickness of this homogeneous stratum.



100

Figure 1. Sedimentary stratigraphy generalization schematic

2.2 Geological structure data

2.2.1 Fold

In nature, fold refers to a stratum that has been subjected to strong forces and structural stress that results in continuous wavy and undulating morphology. The portion of the fold that is bent upwards is called an anticline, and a syncline is where the fold is bent downwards. In general, folds are rarely formed by only one force, and are often the result of at least horizontal or inclined compressional forces and gravity. The formation of folds in nature may involve more complex forces, resulting in a variety of fold forms. Therefore, based on geological terminology, this work selectively simplifies and parameterizes fold structures by using fold elements that describe the shape and occurrence of folds. The basic components of folds (Fig. 2(a)) include: (1) The core of the fold, which indicates the rock layer at the centre of the fold. (2) The limb, which refers to the area where the sides of the fold are relatively straight. (3) The hinge zone, which refers to the curved portion where the two wings of the fold join. Here the morphology can be categorized as circular, sharp-angled, box-shaped and knee-shaped. Additionally, folds can be described, for example, as archlike folds, chevron folds, box folds, fan folds and flexures. (4) The hinge, which refers to the location of maximum bending on the fold surface. Hinges are mostly straight lines but may also be curved or folded lines, and its yield is horizontal, inclined or upright, which represents the variability of the fold along the direction of its extension. (5) The axial plane is where the hinge of the adjacent folded surface is connected to form a hypothetical marker surface, which is mostly flat and straight, but can also be curved. The intersection of the axial plane with the ground or any other plane is called the axial trace. (6) The inflection point is the dividing point between the dorsal and diagonal vectors along the continuous fold waveform, i.e., the point where the curvature of the fold is zero. (7) The apex line (also called the ridge

110

115



120 line) and trough line refer to the lines that connect the highest points of the same anticline and the lowest points of the same syncline, respectively.

We first simplify folds into periodic oscillatory global folds according to the geological characteristics of folds. For the hinge zone, only the more common rounded, pointed prismatic and boxed shapes are considered in this study. This study simplifies the hinge as a straight, horizontally oriented line. Depending on the subsequent tilt of the geological structure, the orientation can be changed to inclined or vertical. This work simplifies the axial plane to a flat surface, and similarly makes the apex and trough lines, straight. Therefore, the fold becomes a periodic fold according to the simplification method, each cycle having the same morphology, and for a single cycle, it is described by the following parameters (Fig. 2(b)): (1) **Height**, which is the vertical distance from the hinge to the inflection point; (2) **Position**, which is the position of the entire fold in the horizontal direction and is represented by the distance of the inflection point from the origin; (3) **Cycle Length**, which is the distance covered by a single cycle in a fold; (4) **Angle**, which is the inclination of the axis surface and is characterized by the angle between the axis surface and the horizontal surface; and (5) **Shape**, which is the shape of the hinge zone and indicates the transition between sharp-angled and box-shaped folds, and the midpoint represents the circular fold.

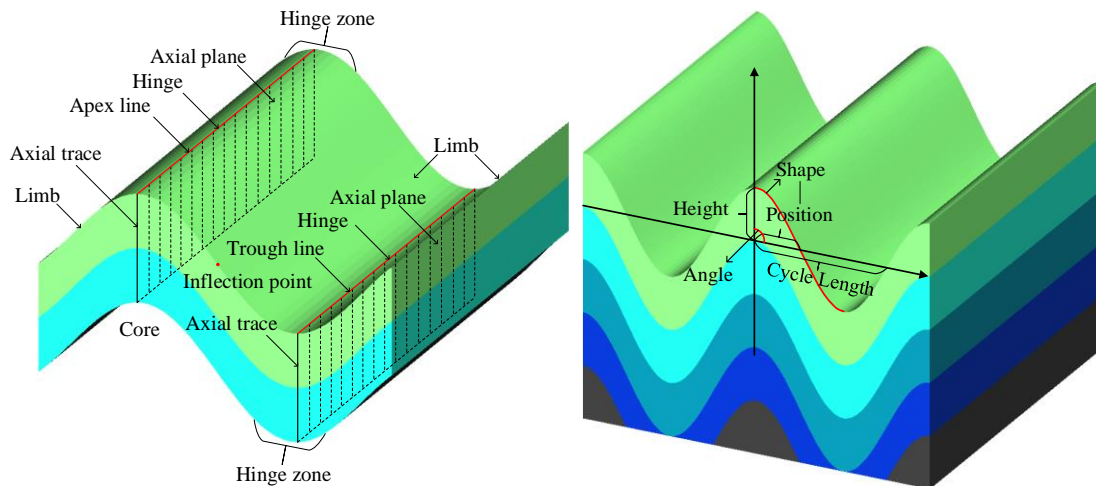


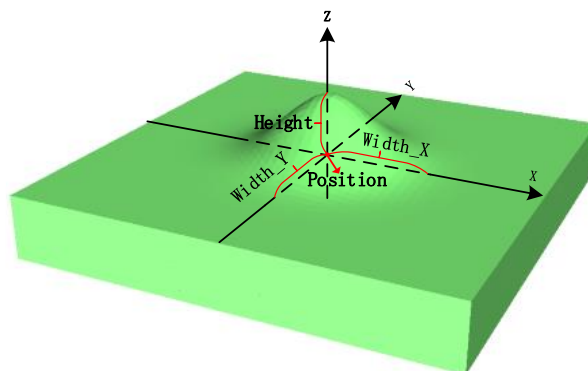
Figure 2. Fold structure generalization schematic. (a) Fold elements; (b) fold parameterization principle.

135 2.2.2 Partial fold

In practice, folds do not necessarily run through the entire study area, thus it is not possible to consider only the global fold. It is also necessary to implement the ability to add a local fold at any position in the study area. In this work, we simplify the partial folds and consider them only as raised or recessed for a distance around the selected position. Therefore, with reference to the definition of the fold parameters, the partial folds are described by the following parameters based on the geological terminology and simplification process (Fig. 3): (1) **Position** refers to the coordinates of the centre of the fold (X , Y) and is used to indicate the position of the added fold; (2) **Height**, which is the vertical distance from the topmost part of this local fold to the Position point; (3) **Width_X**, i.e., the X-direction fold degree parameter, which is the influence range of the partial



fold in the X-direction and is used to indicate the maximum distance of this partial fold in the X-axis direction. (4) **Width_Y**, the Y-direction fold degree parameter, which is defined similarly as Width_X.



145

Figure 3. Partial fold parameterization schematic

2.2.3 Tilt

The tilt structure is a rock formation that has a certain angle between the rock plane and the horizontal plane after the structure changes. If the tilt direction and dip angle of a set of tilted rock formations in a certain area are largely the same, it is called a single-slope structure, which is the simplest form of tilt. There are three main types of tilted structure rock formations: fold structures with only a single wing, a disk of fault structures, or faults caused by uneven uplift or downwards movement in the region. Determining the orientation of tilted rock formations is the basis for studying tilted geological formations. Tilt is determined by measuring the direction of extension of the rock plane in 3D space and the angle with a geodetic level (horizontal plane). Tilt measurements consist of three elements of orientation: strike, dip, and dip angle (Fig. 4). (1) The straight line where the rock layer intersects the horizontal plane is called the strike line, and the direction indicated by the strike line is the direction of the rock layer, which indicates the extension direction of the rock layer in space; (2) Dip refers to the line on the rock formation that is perpendicular to the strike line and extends downwards along the slope (i.e., the true tilt line), and the projection of the true tilt line in the horizontal plane is the strike line, and the direction indicated by the strike line is the tendency of the rock formation; (3) The dip angle is the angle between the true inclination line and the true tilt line.

160 This study simplifies and parameterizes the tilted structure based on the geological characteristics of the tilted structure and the three elements of orientation. First, the tilted structures are reduced to the simplest single-slope structures. Since it is known that the tendency line and the strike line are perpendicular to each other based on the character of the orientation, the following two parameters (Fig. 4) can be used to describe the tilted structures: (1) **Strike angle**: the angle between the strike line and due north represents the orientation of the strike element; (2) **Dip angle**: the angle between the inclination line and the tilt line, which also indicates the angle between the tilted rock formation and the horizontal plane represents orientation of the dip angle.

165

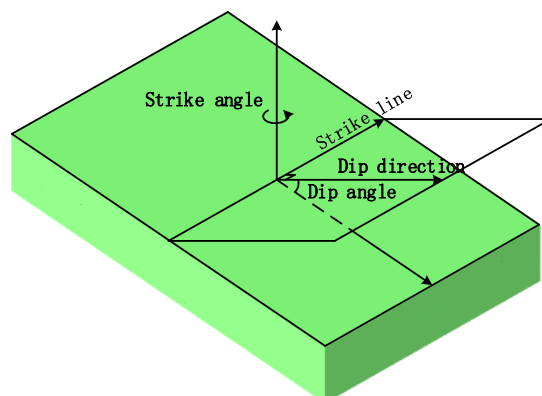


Figure 4. Tilt structure parameterization schematic

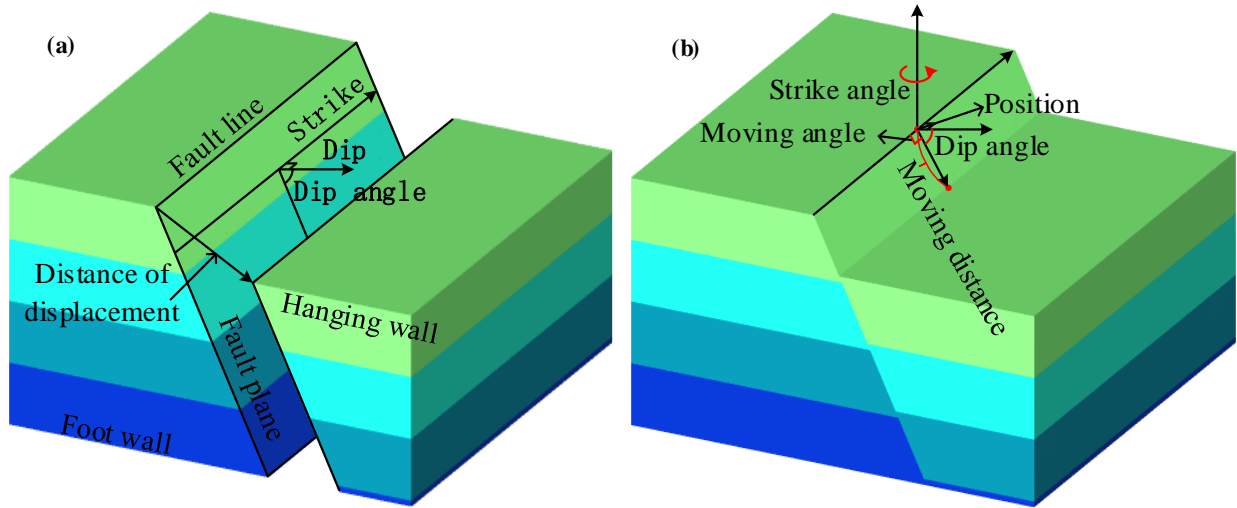
2.2.4 Fault

170 A fault is a geological formation in which a rock layer or a rock body is fractured by force and the rock masses on both sides
are significantly displaced relative to each other along the ruptured surface. Faults are common features in the Earth's crust,
and they vary in size and scale, from large faults extending hundreds to thousands of metres along the strike to small faults of
only a few tens of centimetres. Faults are some of the most important structures related to the movement of the Earth's crust.
Geometric elements of faults are the basis of fault geometry studies and include the fault surface, fault line, fault disk and fault
175 distance (Fig. 5(a)). (1) The fault plane constitutes the ruptured surface of the fault, that is, the surface formed by significant
relative sliding of rock bodies along both sides of the fault. The fault plane is generally composed of a series of rupture surfaces
or secondary fault zones and is, therefore, also called the fault zone or fracture surface. Similarly, we can describe the spatial
location of the fault surface in terms of the three orientation elements. (2) The fault line refers to the intersecting line between
the fault surface and the ground, and the direction of the fault line is the strike of the fault. (3) The Fault wall is the location of
180 relative displacement on both sides of the fault and is divided into the hanging wall and lower foot wall. (4) Distance of
displacement is the distance between the two fault walls and the location of relative sliding along the fault plane. Faults can
be divided into three categories, compressional faults, tensional faults, and torsional faults. Additionally, faults can be
classified according to their mechanical properties and the relative motion of the fault disk; these are normal faults, reversed
faults, parallel faults and hinge faults.

185 We simplify the fault surface into a plane and express its location with three elements of orientation according to the fault
elements and fault classification. We simplify the relative motion of both disks of the fault as translational motion considering
the simplicity of parameter expression. Although all faults in nature have some rotation, the angle is generally not large.
Therefore, only normal faults, reversed faults, parallel faults and their combination of fault types are considered in this work
(Fig. 6). Therefore, the fault can be described by the following parameters (Fig. 5(b)): (1) Orientation parameters, such as the
190 tilted structure, are used to describe the **posture** of the fault, namely, the two variables *Strike angle* and *Dip angle*; (2) *Position*,
the location parameter, is used to describe the centre location of the fault plane in the study area; (3) *Moving angle*, the relative



sliding angle is used to describe the moving direction of the hanging wall relative to the foot wall; and (4) **Moving distance**, i.e., slip distance, which is the distance of fault elements such as the distance between two walls where relative slip occurs.



195 **Figure 5. Fault structure generalization schematic. (a) Fault elements; (b) fault parameterization principle.**

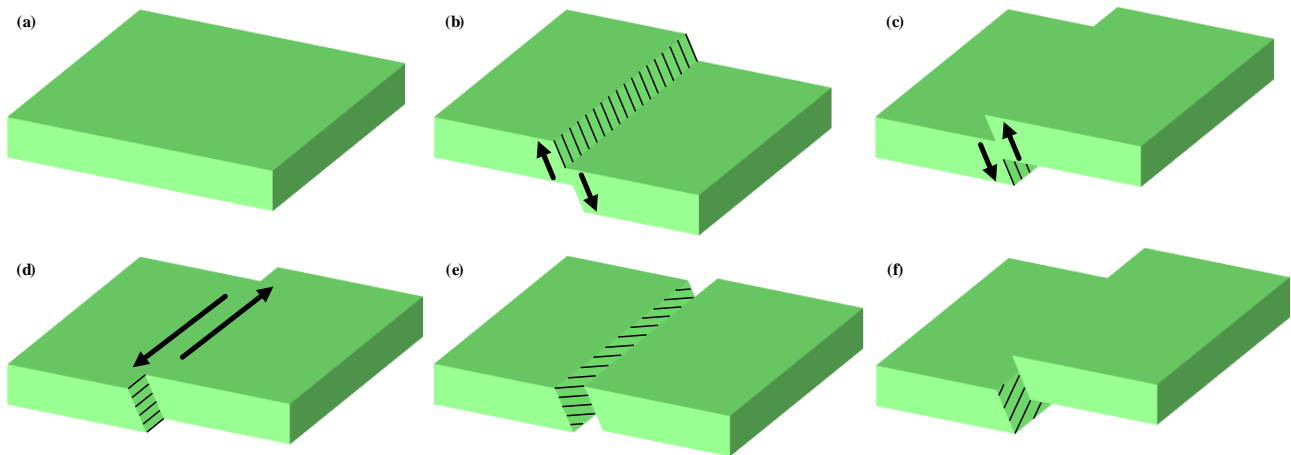


Figure 6. Fault combination type. (a) Normal rock formation; (b) normal fault; (c) reversed fault; (d) parallel fault; (e) parallel normal fault; (f) parallel reversed fault.

2.2.5 Unconformity

200 Unconformities describe stratigraphic relationships between two sets of adjacent strata of different ages above and below where depositional interruptions or stratigraphic deficiencies have occurred. An unconformity is generally classified as being either an angular unconformity or a pseudo-conformity (also known as disconformity). An angular unconformity refers to two sets of strata that are in contact at an angle, and a pseudo-conformity refers to two sets of strata that are in roughly parallel contact. The interface between two sets of strata in contact is called the erosion surface (also called the unconformity surface).



205 We first simplify the contact surface, i.e., the unconformity plane, to a horizontal plane according to the characteristics
of the unconformity, and then the set of strata above the contact surface are simplified according to the simple sedimentary
stratigraphy presented in this paper (2.1). Therefore, the following parameters are used to describe the unconformity structure
(Fig. 7): (1) **Position**, i.e., the height position parameter, refers to the position of the horizontal plane within the model area;
(2) **Number**, i.e., number of strata, refers to the number of layers in a set of sedimentary strata above the contact;
210 refers to the thickness of each layer of a set of sedimentary strata above the contact.

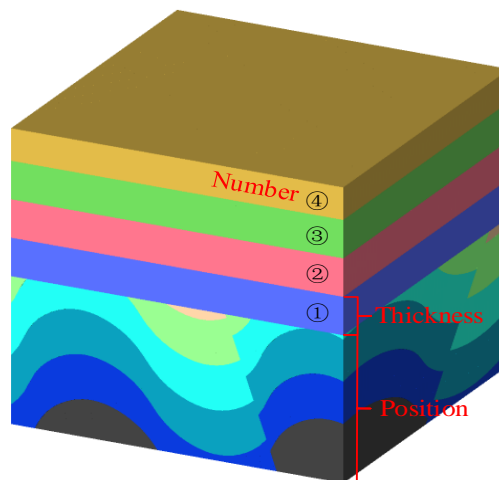


Figure 7. Unconformity parameterization schematic

2.2.6 Intrusive rock

Intrusive rocks refer to the rocks formed when the pressure of the overlying rock layer decreases, and the magma invades the
rock layer or fissures in the crust from below and then gradually cools and solidifies within the earth. Intrusive rocks can be
215 divided into stocks, apophyses, dikes, sheets, and batholiths according to different occurrences. In this study, only stock and
dikes are considered. Since batholiths rarely appear and apophyses are similar **to tree branches (but with more bifurcations)**
and are not easy to simulate, these two categories are not considered at this time. Simulating the other two categories according
to their morphology reveals that the stocks is an unconformable intrusion that extends downwards in a trunk-like pattern on a
220 larger scale while dikes, also known as "rock walls", are a more commonly distributed intrusive vein. Dikes are similar to slab-
like rock filled with rock fissures that cuts across the rock layer and intersects the laminae obliquely, which is a kind of intrusive
unconformity. Therefore, the shape of the dikes is slab-like, and the stock is columnar.

We simplify the dikes into flat plates and the strains into synapses according to the shape of the veins and strains.
Therefore, the following parameters can be used to describe each of these two intrusive rock forms. Dikes (Fig. 8(a)) can be
225 described based on their orientation parameters (i.e., **strike angle** and **dip angle**), **position**, and **thickness**. The strike and dip
angle refer to the tilted structure of the dike and are used to describe the dike posture while the position parameter describes
the central location of the dike and thickness describes the dike thickness. Stocks (Fig. 8(b)) can be described in terms of their



230

position, *radius*, and *height*. The position parameter refers to the planar location of the centroid of the stock. The radius parameter refers to the radius of the bottom end of the stock and is used to describe the extent of the stock while the height parameter describes the maximum elevation to which the rock has intruded.

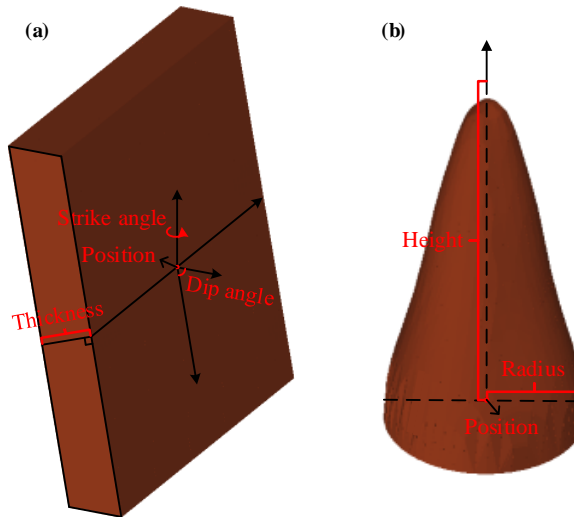


Figure 8. Intrusive rock parameterization schematic. (a) Dikes; (b) Stock.

3 Methodology of structural simulation

3.1 Construct strata

235 The strata are the basis of the whole evolutionary process, and all methodological modules of geological formations are carried out on the strata. Therefore, for the numerical representation of the geological body, a suitable data model is needed. Here we use a tetrahedral model to (Fig. 8) construct the stratigraphic model as opposed to a hexahedral model (Bagley et al., 2016) or other. There are many advantages of organizing within tetrahedral forms compared to other models. (1) First, a tetrahedral raster field can contain more triangular surfaces with the same accuracy and can represent the geological model more precisely.
240 (2) Calculating the intersection of a face with a tetrahedron is much easier. (3) **The tetrahedron can be divided iteratively.** The space of a tetrahedron can be continually divided into two parts, which can still be represented by the tetrahedron. (4) The tetrahedral raster field provides a better structural basis for model analysis and model operators such as arbitrary planar sectioning, excavation in different ways, and volume statistics (Guo et al., 2021). The above advantages provide the possibility of repeatedly adding geological formations, ensuring that regardless of the operation being carried out, the whole model is still
245 represented by tetrahedron.

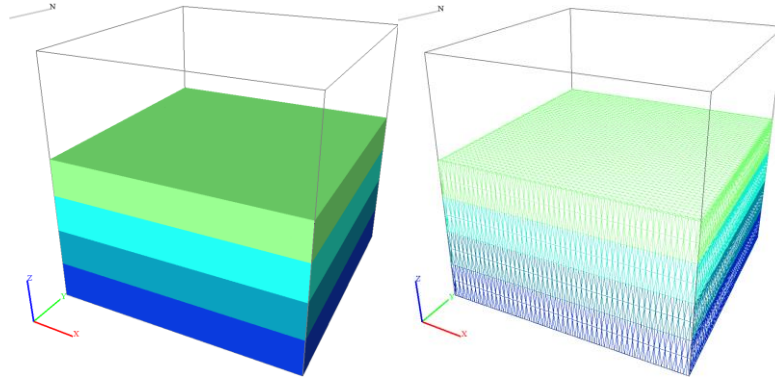


Figure 9. **Tetrahedral raster construction stratigraphic model**

3.2 Fold

3.2.1 Global fold

250 In the 3D geological model, we simulate the folding action by introducing a vertical shear model. The shear action is defined by the combination of displacement field $S_1(X, Y, Z)$ and rotational field $R_z(X, Y, Z)$. Considering the different forms of folds (mainly archlike folds, chevron folds and box folds are considered), the displacement field is defined as a complex superposition of three functions. The archlike fold is defined as a cosine function $f_1(X, Y, Z)$ (Eq. (1)), the chevron fold is defined as a jagged segmented periodic function $f_2(X, Y, Z)$ (Eq. (2)), and the box fold is defined as a segmented combined
 255 higher-order periodic function $f_3(X, Y, Z)$ (Eq. (3)).

$$f_1(X, Y, Z) = A \cos(\omega X + \varphi) \quad (1)$$

$$f_2(X, Y, Z) = \begin{cases} \frac{2A\omega}{\pi} \left(X - \frac{2k\pi}{\omega} + \varphi \right) + A & \left[(2k-1)\frac{\pi}{\omega}, 2k\frac{\pi}{\omega} \right) \\ -\frac{2A\omega}{\pi} \left(X - \frac{(2k+1)\pi}{\omega} + \varphi \right) + A & \left[2k\frac{\pi}{\omega}, (2k+1)\frac{\pi}{\omega} \right) \end{cases} \quad k = 0, 1, 2, 3, \dots \quad (2)$$

$$f_3(X, Y, Z) = \begin{cases} A \left(\frac{2\omega}{\pi} \right)^6 \left(X - \frac{(4k-3)\pi}{2\omega} + \varphi \right)^6 - A & \left[(2k-1)\frac{\pi}{\omega}, (2k-1)\frac{\pi}{\omega} + \frac{\pi}{2\omega} \right) \\ -A \left(\frac{2\omega}{\pi} \right)^6 \left(X - \frac{(4k+1)\pi}{2\omega} + \varphi \right)^6 + A & \left[(2k-1)\frac{\pi}{\omega} + \frac{\pi}{2\omega}, (2k+1)\frac{\pi}{\omega} - \frac{\pi}{2\omega} \right) \\ A \left(\frac{2\omega}{\pi} \right)^6 \left(X - \frac{(4k+4)\pi}{2\omega} + \varphi \right)^6 - A & \left[(2k+1)\frac{\pi}{\omega} - \frac{\pi}{2\omega}, (2k+1)\frac{\pi}{\omega} \right) \end{cases} \quad k = 0, 1, 2, 3, \dots \quad (3)$$

where A , ω , and φ are chosen within a certain range and these three parameters represent the height of the fold, the degree of
 260 the fold, and the position of the fold. Then, f_1 , f_2 , and f_3 are combined by a shape parameter δ in the range $[-1, 1]$ to obtain the shearing fields $S_0(X, Y, Z)$ where -1 represents the chevron folds, 0 represents the archlike folds, 1 represents the box shape, and the shapes are combined using Eq. (4).

$$S_0(X, Y, Z) = \begin{cases} -\delta * f_2(X, Y, Z) + (1 + \delta) * f_1(X, Y, Z) & \delta \in [-1, 0] \\ \delta * f_3(X, Y, Z) + (1 - \delta) * f_1(X, Y, Z) & \delta \in (0, 1] \end{cases} \quad (4)$$



Then, the simulation of the fold axial plane angle α is realized by using the combination of the plane function $f_4(X, Y, Z)$ (Eq. (5)) and the rotation fields \mathcal{R}_Y and S_0 . First, S_0 and f_4 are combined to obtain the final displacement field S_1 according to Eq. (6), then the rotation of the axial plane angle is realized using the rotate field \mathcal{R}_Y (Eq. (7)).

$$f_4(X, Y, Z) = (\tan \alpha)X \quad (5)$$

$$S_1(X, Y, Z) = S_0(X, Y, Z) + f_4(X, Y, Z) \quad (6)$$

$$\mathcal{R}_Y(\theta_Y) = \begin{bmatrix} \cos \theta_Y & 0 & \sin \theta_Y \\ 0 & 1 & 0 \\ -\sin \theta_Y & 0 & \cos \theta_Y \end{bmatrix} \quad (7)$$

where $\mathcal{R}_Y(\theta_Y)$ is a 3D rotation matrix rotated about the Y axis and θ_Y is the rotation angle around the Y axis. Using this rotation field to rotate the final displacement field $S_1(X, Y, Z)$ by the $-\alpha$ angle around the Y axis, i.e., $S_1(X, Y, Z) * \mathcal{R}_Y(-\alpha)$, the axis plane is successfully tilted by the α angle. This displacement field is only used to create the shape of the fold along the X-direction.

However, the above methods can only simulate folds along the X-direction and cannot simulate folds in any other direction. Therefore, this study further makes use of the rotation equation around the Z-axis (Eq. (8)) to enable the folds to be added in any direction.

$$\mathcal{R}_Z(\theta_Z) = \begin{bmatrix} \cos \theta_Z & -\sin \theta_Z & 0 \\ \sin \theta_Z & \cos \theta_Z & 0 \\ 0 & 0 & 1 \end{bmatrix} \quad (8)$$

The rotation field is a 3D rotation matrix rotating around the Z-axis, and θ_Z is the angle around the Z-direction, chosen within a certain range. Here we construct the following rotation field $R_z(X, Y, Z)$ (Eq. (9)) using the rotation matrix so that the axes of the rotation field translate to the centre point of the model (X_c, Y_c, Z_c) . The rotational field is used in several subsequent constructions and will not be frequently repeated.

$$R_z(X, Y, Z) = \mathcal{R}_z(\theta_z) \begin{bmatrix} X - X_c \\ Y - Y_c \\ Z \end{bmatrix} + \begin{bmatrix} X_c \\ Y_c \\ 0 \end{bmatrix} \quad (9)$$

Using the combination of the shear displacement field $S_1(X, Y, Z)$ and the rotation field $R_z(X, Y, Z)$ in Eq. (10), we can add a fold structure to the original geological model (Fig. 10(a), (X, Y, Z) in Eq. (10)) to obtain a new folded geological model (Fig. 10(e)(f)(g), $(\tilde{X}, \tilde{Y}, \tilde{Z})$ in Eq. (10)).

$$\begin{bmatrix} \tilde{X} \\ \tilde{Y} \\ \tilde{Z} \end{bmatrix} = \begin{bmatrix} X \\ Y \\ Z + S_1(X, Y, Z) * \mathcal{R}_Y(-\alpha) \end{bmatrix} * R_z(X, Y, Z) \quad (10)$$

Fig. 10(b)(c)(d) shows the fold preview morphology of the fold model (Fig. 10(e)(f)(g)). We can clearly see the pattern of the fold to be added. By choosing the displacement field parameters A , ω , φ , and α and the rotation field parameter θ , we



can add any overall fold configuration with different bending structures that we need to the model. In Fig. 10, panels (b)(e),
 290 (c)(f) and (d)(g) are the fold surface preview and fold simulation results of archlike folds, chevron folds and box folds,
 respectively.

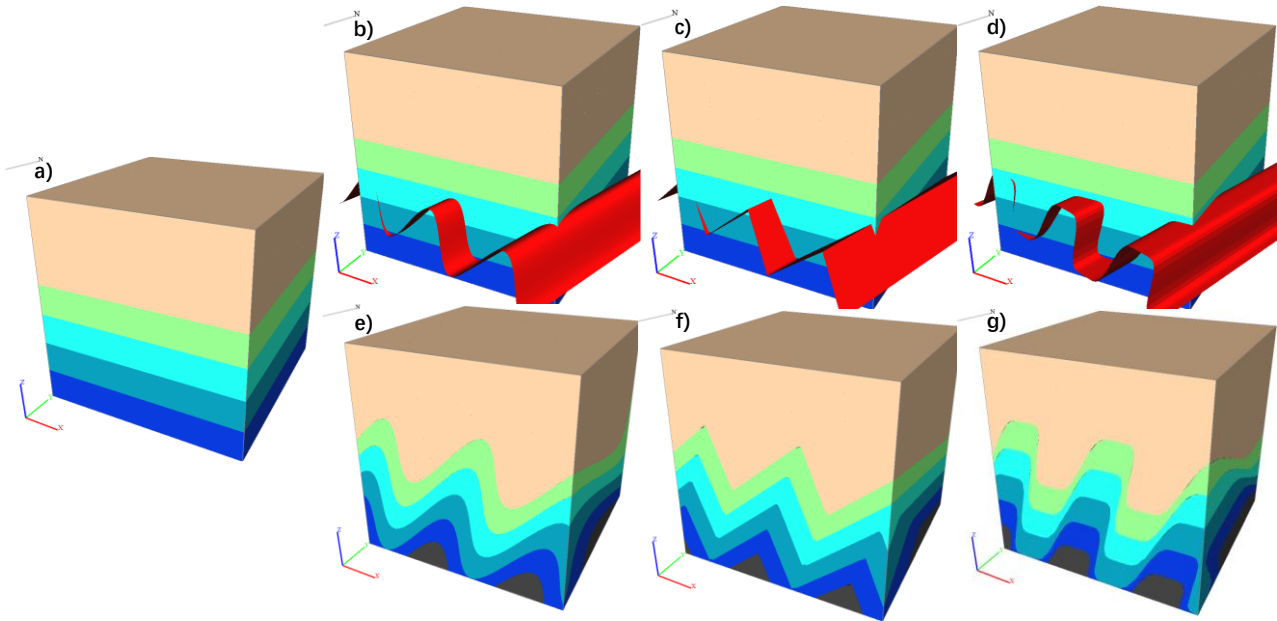


Figure 10. The fold structure effect. (a) Original geological model; (b) archlike fold preview; (c) chevron fold preview; (d) box fold preview; (e) archlike fold result model; (f) chevron fold result model; (g) box fold result model.

295 3.2.2 Partial fold

We have implemented the fold module, but the fold module runs through the overall model. In fact, folds generally do not
 occur evenly in the whole study area according to the different geological characteristics, but there will be partial folds.
 Therefore, the global folding module alone is not sufficient for the evolution of most geological situations. Therefore, in this
 study, the Gaussian function Eq. (11) is used to propose the local translation field $S_2(X, Y, Z)$ to realize the partial fold module
 300 (Wu et al., 2020) according to the morphology of the partial fold definition.

$$S_2(X, Y, Z) = A \exp \left\{ - \left[\frac{(X-X_0)^2}{2\sigma_x^2} + \frac{(Y-Y_0)^2}{2\sigma_y^2} \right] \right\} \quad (11)$$

where A , σ_x , and σ_y are selected within a certain range as parameters to control the form of the partial fold, A controls the
 pleat height, and σ_x and σ_y control the degree of pleat intensity in the X and Y directions; the larger the fold is, the more
 intense. (X_0, Y_0) is the centre point of the fold, and the default is the centre point of the model but can also be replaced by
 305 selected points. Therefore, the translation field realized by this method can add local folds along the X direction or Y direction.

Similarly, the rotational field is further utilized to enable the addition of local folds in any direction. The rotational field
 is detailed in Eq. (9) and will not be repeated here.



Combining the above displacement field $S_2(X, Y, Z)$ and rotation field $R_z(X, Y, Z)$, we obtain Eq. (12). Therefore, by using Eq. (12), we can add a fold structure to the original geological space (Fig. 11(a)). (X, Y, Z) in Eq. (12)) is used to obtain a new folded geological space (Fig. 11(c)), $(\tilde{X}, \tilde{Y}, \tilde{Z})$ in Eq. (12)).

$$\begin{bmatrix} \tilde{X} \\ \tilde{Y} \\ \tilde{Z} \end{bmatrix} = \begin{bmatrix} X \\ Y \\ Z + S_2(X, Y, Z) \end{bmatrix} * R_z(X, Y, Z) \quad (12)$$

Fig. 11(b) shows a preview of the partial fold. By the above method, we can add different morphological structures to the model at any position we need for local fold construction. With the above methods, we can add partial folds of different morphologies and structures to the model at any position.

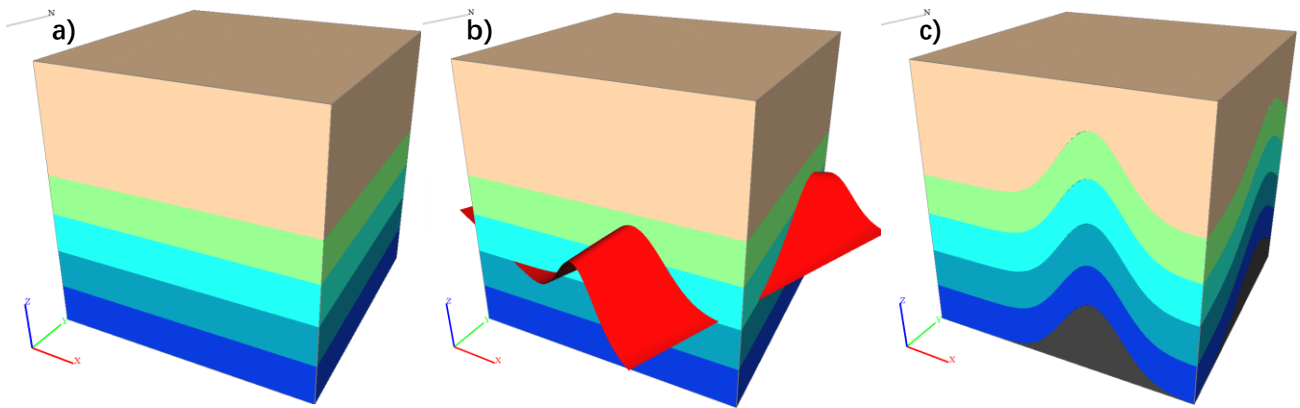


Figure 11. Adding the partial fold. (a) Original geological model; (b) partial fold preview; (c) partial fold result model.

3.3 Tilt

The stratigraphic tilt structure is realized by rotating the 3D structural model, and the rotation angle, i.e., the tilt angle of the model, is determined by two angles or rotation around one Z-axis (rotation matrix Eq. (8)) and one Y-axis (rotation matrix Eq. (13)).

$$\mathcal{R}_y(\theta_y) = \begin{bmatrix} \cos \theta_y & 0 & \sin \theta_y \\ 0 & 1 & 0 \\ -\sin \theta_y & 0 & \cos \theta_y \end{bmatrix} \quad (13)$$

The overall 3D model is then rotated around the centre of the model to achieve the desired angle by the two rotation fields (Eq. (9) and Eq. (14)). The principle is similar to that of the partial fold rotation field, which is not repeated here.

$$R_y(X, Y, Z) = \mathcal{R}_Y(\theta_Y) \begin{bmatrix} X - X_c \\ Y \\ Z - Z_c \end{bmatrix} + \begin{bmatrix} X_c \\ 0 \\ Z_c \end{bmatrix} \quad (14)$$



325 By rotating the two rotation fields $R_z(X, Y, Z)$ and $R_y(X, Y, Z)$ along the axis of the model midpoint (Eq. (15)), a new tilted 3D geological structure (Fig. 12(c), $(\tilde{X}, \tilde{Y}, \tilde{Z})$ in Eq. (15)) can be obtained by adding a tilted structure from any angle to the original 3D geological structure (Fig. 12(a), (X, Y, Z) in Eq. (15)).

$$\begin{bmatrix} \hat{X} \\ \hat{Y} \\ \hat{Z} \end{bmatrix} = \mathcal{R}_z(\theta_z) \begin{bmatrix} X - X_c \\ Y - Y_c \\ Z \end{bmatrix} + \begin{bmatrix} X_c \\ Y_c \\ 0 \end{bmatrix}, \begin{bmatrix} \tilde{X} \\ \tilde{Y} \\ \tilde{Z} \end{bmatrix} = \mathcal{R}_z(\theta_z) \begin{bmatrix} \hat{X} - X_c \\ \hat{Y} \\ \hat{Z} - Z_c \end{bmatrix} + \begin{bmatrix} X_c \\ 0 \\ Z_c \end{bmatrix} \quad (15)$$

330 Fig. 12(b) shows a preview of the surface of the tilt angle. By combining the above method with the tetrahedral raster field, the addition of the tilted geological structure can be realized while ensuring that the topological relationship remains unchanged.

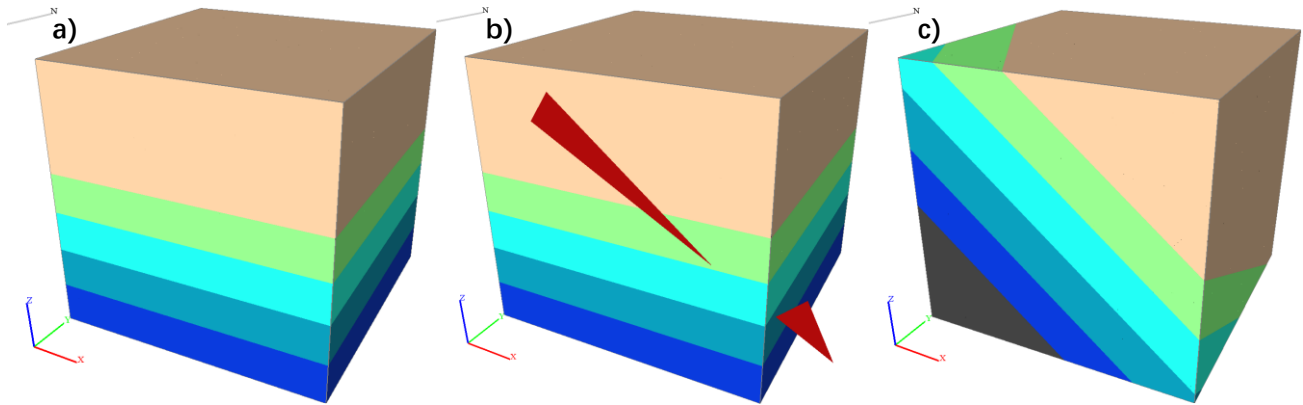


Figure 12. Adding the tilt effect. (a) Original geological model; (b) tilt preview; (c) tilt result model.

3.4 Fault

335 Faults are an important type of geologic structure. Here we use the moving tetrahedron method (Guo et al., 2021) to cut the stratigraphy within the tetrahedron grid field according to the specified fault plane. Then, the two parts obtained after the division are interwoven to simulate the fault. In order to make the selection of parameters more intuitive, we use a plane (Eq. (16)) parallel to the y-axis and a rotational field (Eq. (9)) rotating around the z-axis to determine the appropriate fault plane.

$$f_1(X, Y, Z) = a(X - X_c) + Z_c + b \quad (16)$$

340 where a is the slope of the plane, determined by the dip of the fault plane, and b is the location parameter of the fault plane, which can change the spatial location of the fault plane. The rotation field can rotate the fault surface to the corresponding angle according to the strike and dip of the fault plane; therefore, the plane can express the fault plane at any angle and the fault structure can move in any direction. Then, adding another rotational field on the fault plane can change the displacement direction of fault.

345 Additionally, a point $p(X_o, Y_o, Z_o)$ on the fault plane and a vector $\vec{m}(x_m, y_m, z_m)$ parallel to the X-O-Z plane and the fault plane (the vector orientation varies with the rotation angle of the selected rotation field on the fault plane and defaults to a



downwards orientation) and a vector $\vec{n}(x_n, y_n, z_n)$ normal to the fault plane at that point are obtained before the parameters of the fault plane are selected. The point p and the two normal vectors vary accordingly with the selected fault surface parameters so that the point p is always on the surface, \vec{m} is always along the fault surface, and \vec{n} is always normal to the fault surface.

350 Furthermore, before selecting each parameter of the fault plane, we define point $p(X_o, Y_o, Z_o)$ on the fault plane, a vector $\vec{m}(x_m, y_m, z_m)$ across point p and parallel to the X-O-Z plane and the fault plane, and a normal vector $\vec{n}(x_n, y_n, z_n)$ of the fault plane across point p . The point p and the two vectors vary accordingly with the selected fault plane parameters, ensuring that the point p is always on the surface, \vec{m} is always along the fault surface and \vec{n} is always the normal vector of the **fault plane**.

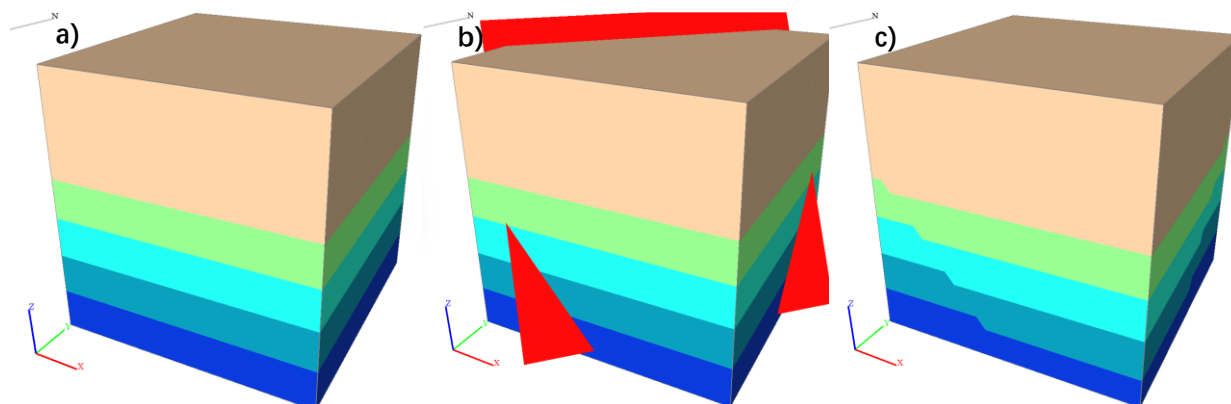
355 After the parameters of the fault surface are determined, the point p on the fault surface and the two vectors are also determined. Then, point p and normal vector \vec{n} are brought into the following equation (Eq. (17)) to obtain the point normal expression.

$$f_2(X, Y, Z) = x_n(X - X_o) + y_n(Y - Y_o) + z_n(Z - Z_o) = 0 \quad (17)$$

After obtaining the equations of the fault surface, we used the moving tetrahedron method to divide the 3D geological structure organized by the tetrahedral grid field into two parts according to the fault surface; part 1 is above the fault surface and part 2 is below. Then, the whole of part 1(X_u, Y_u, Z_u) is moved along the direction of vector \vec{m} by a distance δ (entered when selecting each parameter of the fault plane) to obtain $(\widetilde{X}_u, \widetilde{Y}_u, \widetilde{Z}_u)$ (Eq. (18)). The direction of \vec{m} is downwards by default, which in this work indicates a normal fault. The $-\vec{m}$ vector is used if a reversed fault is selected. Though this can also be modified according to the rotation angle of the rotational field located on the plane to achieve different directions and thus simulate a walking slip fault. Finally, the two parts are combined by stratigraphic correlation to obtain the final fault model.

$$\begin{bmatrix} \widetilde{X}_u \\ \widetilde{Y}_u \\ \widetilde{Z}_u \end{bmatrix} = \begin{bmatrix} X_u \\ Y_u \\ Z_u \end{bmatrix} + (-)\delta \begin{bmatrix} x_m / \sqrt{x_m^2 + y_m^2 + z_m^2} \\ y_m / \sqrt{x_m^2 + y_m^2 + z_m^2} \\ z_m / \sqrt{x_m^2 + y_m^2 + z_m^2} \end{bmatrix} \quad (18)$$

Using the above method, we can obtain a new geological structure (Fig. 13(c)) after simulating the occurrence of normal or reverse faults at any location of the original geological structure (Fig. 13(a)), where Fig. 13(b) is a preview of the surface when selecting the location of the fault plane.



370

Figure 13. Adding the fault. (a) Original geological model; (b) fault preview; (c) fault result model.

3.5 Unconformity

Stratigraphic unconformities are also an important and frequently occurring structural phenomenon, and it is necessary to understand the underlying causes before simulating them. The development of unconformity surfaces starts with the deposition of older strata, followed by crustal movement and the exposure of older strata to surface erosion, and finally the deposition of newer strata according to the principle of unconformity structure parameterization above. Simply put, the surface is eroded first and then material is subsequently deposited.

375

Therefore, following this feature, we use a similar method to add a series of new sedimentary strata to the original geomorphic body. However, the model is cut at the location of the additions using a method that simulates the fault structure before adding the unconformity, and only the lower part is retained to simulate denudation. The cutting operation simply divides the original geological body at the location where stratigraphy will be added using a plane parallel to X-O-Y. The detailed procedure is described in the simulated faults section and will not be described here.

380

By using this cut-then-add method, we can simulate a simple unconformity within the original geological structure (Fig. 14(a)) to obtain a new 3D geological structure (Fig. 14(c)). Fig. 14(b) shows a preview of the added unconformity, and we can preview and modify the location, number of strata and thickness of the strata to be added.

385

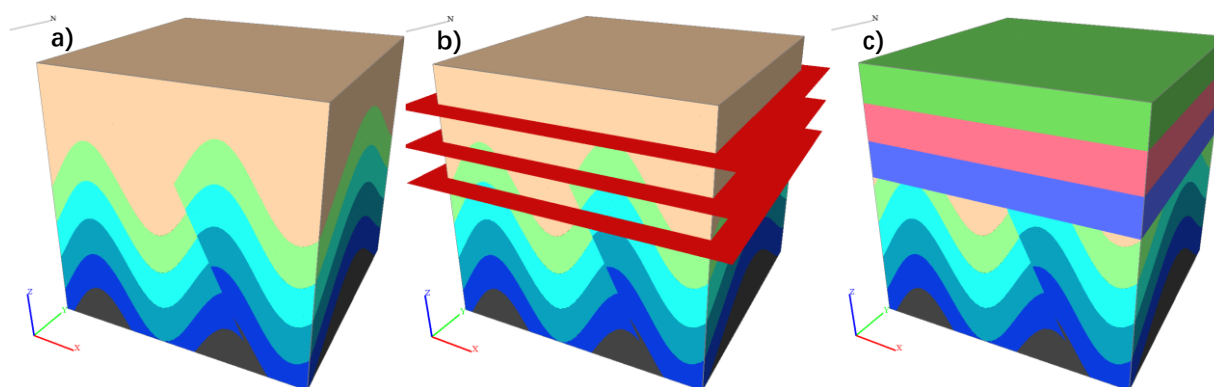


Figure 14. Adding the unconformity. (a) Original geological model; (b) unconformity preview; (c) final unconformity model result.



3.6 Intrusive rock

We use two parallel planes $f_1(X, Y, Z)$ (Eq. (19)) and $f_2(X, Y, Z)$ (Eq. (20)) with δ intervals to represent the dike and use one
 390 Gaussian plane $f_3(X, Y, Z)$ (Eq. (21)) to represent the stock according to the shape characteristics of the dike and stock
 discussed above. Cutting twice using the two parallel planes to obtain a model body of a certain thickness, and then the
 geological properties of this model body were changed to an intrusive dike. The Gaussian surface is used to simulate the stock
 thereby dividing the model using the Gaussian surface to obtain a columnar body and similarly changing the geological
 properties of this geological body to reflect the intrusive stock.

$$395 \quad f_1(X, Y, Z) = a(X - X_c) + Z_c + b - \frac{\delta}{2} \quad (19)$$

$$f_2(X, Y, Z) = a(X - X_c) + Z_c + b + \frac{\delta}{2} \quad (20)$$

$$f_3(X, Y, Z) = A \exp \left\{ - \left[\frac{(X - X_0)^2 + (Y - Y_0)^2}{2\sigma^2} \right] \right\} \quad (21)$$

By using the above two simple functions to cut and then change the properties, we can successfully add the intrusive dike
 or stock to the original geological structure (Fig. 15(a)) to obtain a new geological body (Fig. 15(c)(e)), where (c) is a dike and
 400 (e) is a stock). Fig. 15(b)(d) shows the preview of intrusive rocks to be added, which can be added according to the change in
 parameters such as location and morphology of the intrusive rocks.

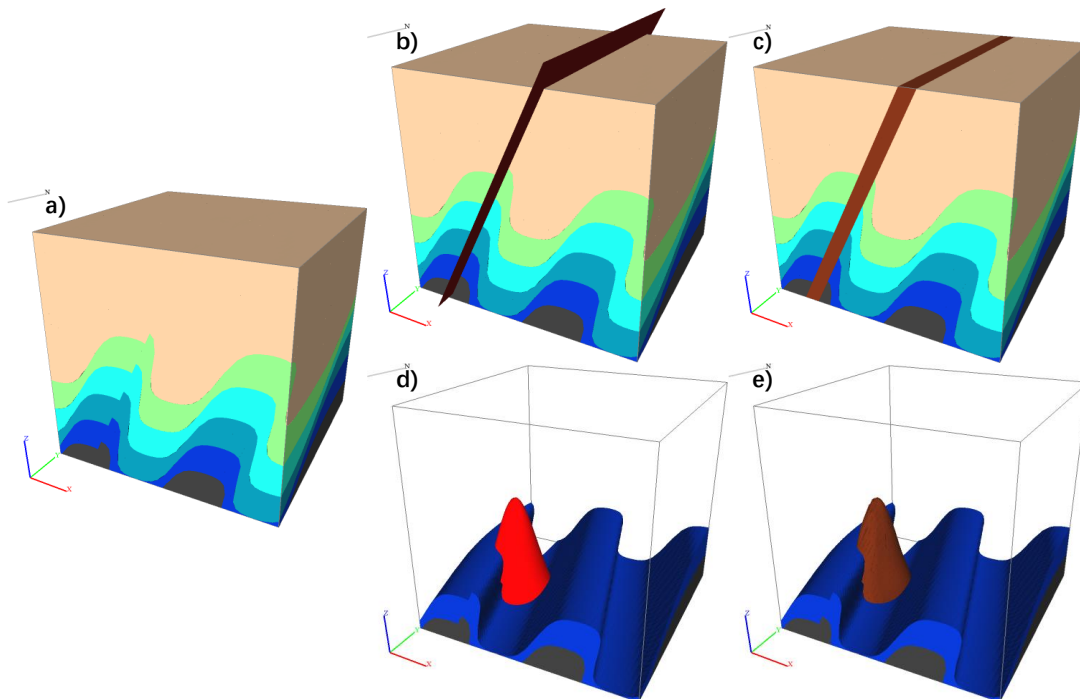


Figure 15. Adding the intrusive rock (dike and stock). (a) Original geological model; (b) intrusive dike preview; (c) intrusive stock preview; (d) intrusive dike result model; (e) intrusive stock result model.



405 4 Case study

We developed a 4D geological structure evolution vector modelling program using the **Qt framework** based on the simulation method presented in this work. Then, we conducted the following case studies using this software. The geological models obtained from the simulations in this section were constructed using a laptop computer (AMD Ryzen9 5900HX 3.3 GHz, 16 GB of RAM, and an NVIDIA GeForce RTX 3060). Case 1 simulates the construction of a complex geological structure based on a series of geological events; Case 2 selects six typical geological features in the world and simulates their evolutionary processes. First, we infer the historical evolutionary process of typical complex geological formations, and then simulate the evolutionary process by using the method developed by this study. Finally, each geological event and corresponding geological model can be clearly viewed according to the historical timeline provided by the model to reveal the 4D reconstruction of geological features. Thus, the formation process of complex geological structures in the region can be intuitively and clearly understood. **We can also store the final modelled processes for review or further modification and editing.**

410

415

4.1 Case 1: Simulation of complex regional geological and structural evolutionary processes

If we want to study the evolutionary process of features in complex regions with many different types of geological structures, we generally deconstruct the existing geology from a geological profile (Fig. 16), which requires not only strong professional knowledge but also a certain degree spatial approximation. It is also difficult to extrapolate feature evolution moving forward through time according to the information within the geological section.

420

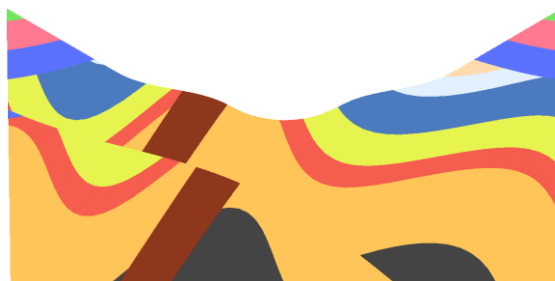


Figure 16. Deconstruction using geological sections.

In contrast, using the forwards simulation software presented in this paper, it is easy to construct historical geological events according to feature evolution. Combining the temporal dimension and the process of regional structure development, the model clearly and visually shows the forms of interaction between new geological events and pre-existing geology and structures. For example, the existing regional geological history was developed from a series of stratigraphic depositional events, folding, tilting, unconformities, diking, faulting, and stocking. The results of a series of events simulated using the geological evolution modelling program presented in this paper are shown in Fig. 17. The software presented here also has different built-in terrain functions, including flat land, hills, ridges, valleys, and cliffs, and we choose the valley terrain in this case (Fig. 17(i)).

425

430

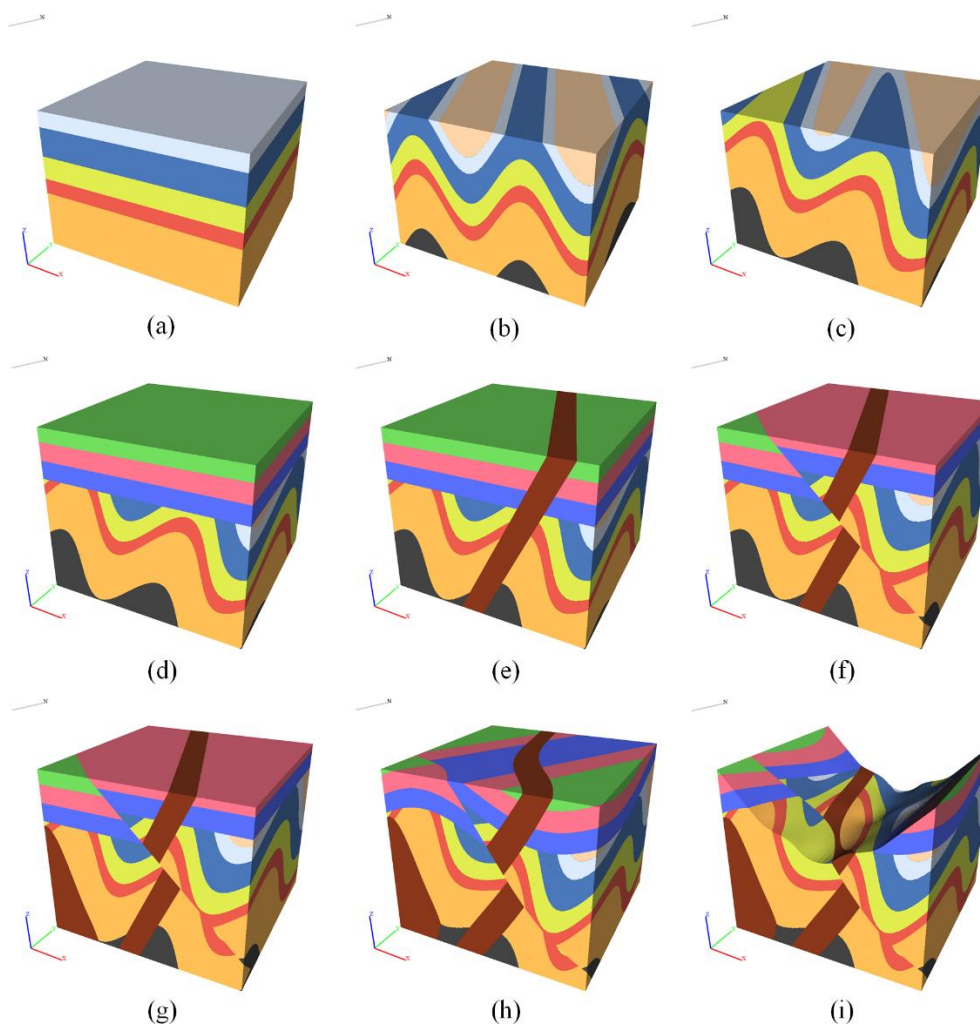


Figure 17. Complex regional geological and structural evolutionary process simulation results. (a) Strata; (b) fold; (c) tilt; (d) unconformity; (e) dike; (f) fault; (g) stock; (h) fold; (i) valley terrain.

Based on the simulation results, it can be concluded that this method can sufficiently simulate the evolutionary process
435 of complex geological structures. It is easy to add various geological events using the methods outlines in this article due to
the modularity of the model process. The user can add arbitrary construction events based on the inferred historical evolution
and check the correctness of the inferred evolution based on the results of the combined events. This can only be achieved in
a simulation that progresses forwards through time, because we can clearly see the effect of each process in the subsequent
geological formations that overprint on the previous geological formations. For example, in Fig. 18(a)(b), the folded and tilted
440 geological structure is folded in front and tilted at the back. The effect is different if the tilt is in front and the fold is behind,
e.g., Fig. 18(c)(d).

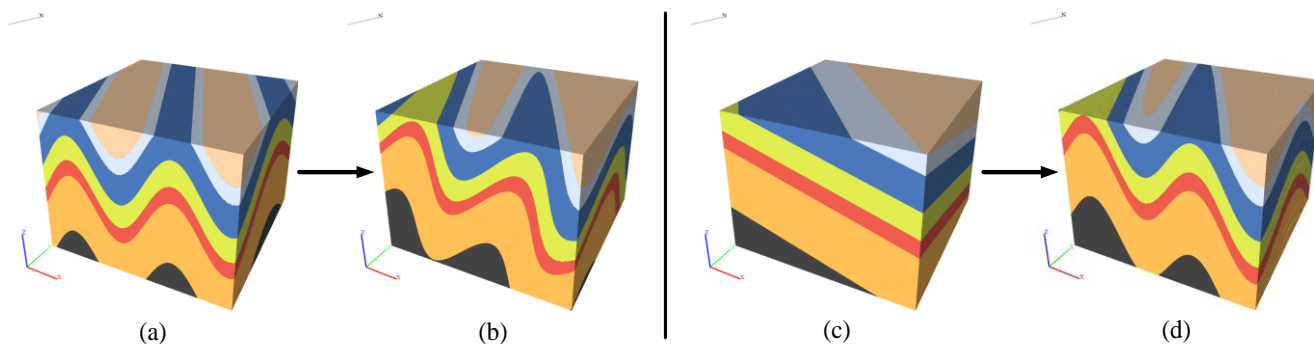


Figure 18. Different sequences of geologic structural development and the influence on the results. (a)(b) The tilted structure occurs after the folded structure; (c)(d) the tilted structure occurs in front of the folded structure.

445 The software also provides the ability to view the history of the model in series via the model timeline and freely creates sections after generating the final model. Thus, it is possible to view the historical evolution of the model dynamically (Fig. 19) by bringing up the model timeline. The timeline records each geological event that affected the model and the time it occurred (user inputs, such as time node shown in Table 1, can be changed.) It can help people more intuitively understand the correlation between 2D sections and 3D geological event processes when combined with the function of generating
 450 corresponding sections by freely selecting two points on the final model.

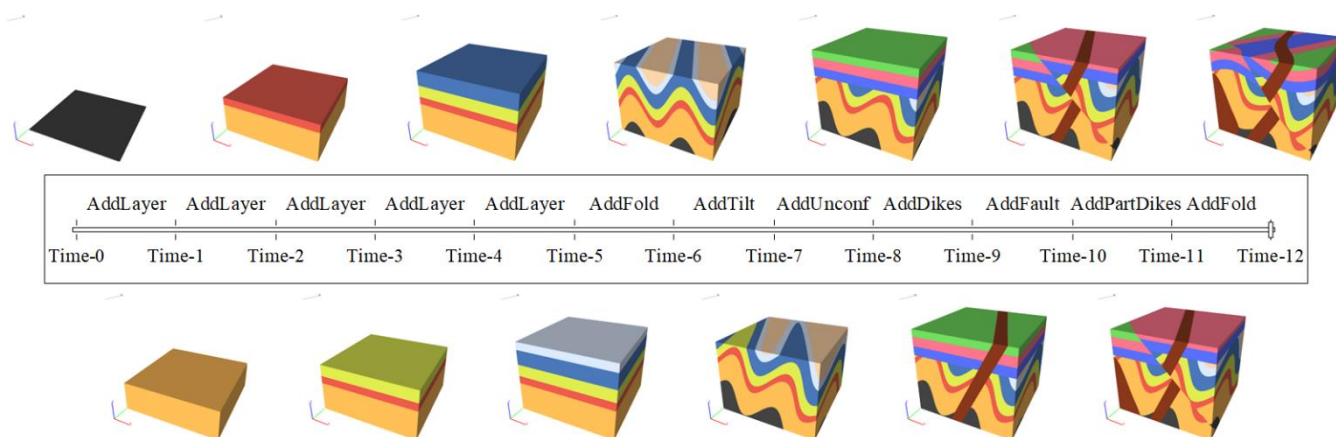


Figure 19. Timeline of regional geological and structural evolutionary history.

Finally, the model's geologic event process also supports saving and importing, allowing the user to save the entire historical evolution of the final model (i.e., each geologic event affecting the model) as a historical process table file (Table 1) and the software supports reopening the file to easily reproduce the evolutionary process. This means that if only the data for a geological event are available, we can generate simulation results by directly inputting these deterministic results into the file. Furthermore, we can fine tune the saved evolutionary process file to quickly modify the parameters of a particular geological event and we can also automatically generate table files via scripting to enable rapid generation of a great quantity simulated geological models.



460

Table 1. Table of historical processes.

Event ID	Event Name	Time Node	Structure Parameters
0	Original	Time-0	null
1	AddLayer	Time-1	layer-1, 30.000, 227.000, 161.000, 67.000
2	AddLayer	Time-2	layer-2, 8.000, 202.000, 71.000, 58.000
3	AddLayer	Time-3	layer-3, 12.000, 190.000, 201.000, 60.000
4	AddLayer	Time-4	layer-4, 15.000, 56.000, 96.000, 156.000
5	AddLayer	Time-5	layer-5, 8.000, 186.000, 198.000, 216.000
6	AddFold	Time-6	0.000, 50.000, 14.000, 22.000, 0.000, 0.000
7	AddTilt	Time-7	40.000, 20.000
8	AddUnconf	Time-8	4.000, 9.000, 60.000
9	AddDikes	Time-9	-160.000, 65.000, 50.000, 10.000
10	AddFault	Time-10	45.000, 54.000, 35.000, 0.000, 15.000, 0.000
11	AddPartDikes	Time-11	0.000, 0.000, 15.000, 15.000, 70.000
12	AddFold	Time-12	0.000, 100.000, 10.000, -30.000, 0.000, 0.000

4.2 Case 2: Simulating the evolutionary process of typical geological features

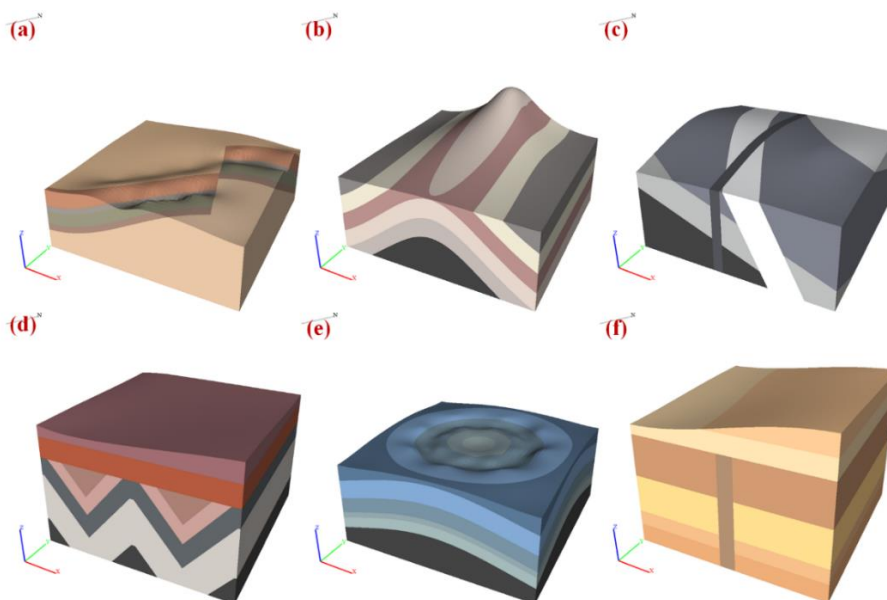
The simulation software presented in this work was used to simulate typical geological features from six geologic sites from around the world (Fig. 20). They are as follows: (a) The Piqiang Fault, which is located in the Tarim Basin of Xinjiang in China. This is a northwest-trending strike-slip fault, in which the reddish, greenish, and brownish bands are continental
 465 Devonian sandstones, Silurian deeper marine sediments and Cambro-Ordovician limestones, respectively. (b) The Sheep Mountain in Wyoming, USA, which is a partially folded structure with harder sandstones within that is cut into ridges, while the weaker shales around them are eroded (Bellahsen et al.). (c) Kosterhavet National Park on Yttre Ursholmen Island in the Koster Islands in Sweden contains multiple stages of pyrogenic intrusion. An igneous intrusion is first cut by a pegmatite dike, which in turn is cut by a dolerite dike. (d) Located in Telheiro Beach in Portugal is a typical angular geologic unconformity
 470 positioned between the schists and metagreywackes of the “Brejeira Formation” from the Upper Carboniferous and new red sandstones of the “Grés de Silves Formation” from the Triassic. (e) The Richat Structure, also named the “Eye of the Sahara”, is a prominent circular geological feature in the Sahara's Adrar Plateau. Initially, it was thought to be caused by a meteorite impact, but it lacked the impact signature of a subsidence ring and evidence of stratigraphic overturning, thus, the possibility of a meteorite impact was negated. However, other scholars thought it was caused by a volcanic eruption, but this theory was
 475 also rejected because of the lack of volcanic rock or a dome of igneous rocks. Currently, academics generally agree that it is a highly symmetrical and deeply eroded geological dome (Matton et al., 2014). (f) Located in Makhtesh Ramon in the Negev



Desert in Israel is a feature formed by a dike and unconformities. Additionally, the area is recognized as a heritage site by the Council for Conservation of Heritage Sites in Israel.



480 **Figure 20. Geologic sites and typical features.** Figure source: (a). [File:Piqiang Fault, China detail.jpg - Wikimedia Commons](#); (b). [Ancient River Channel & Sheep Mountain - Geology of Wyoming \(geowvo.com\)](#); (c). [File:Multiple Igneous Intrusion Phases Kosterhavet Sweden.jpg - Wikimedia Commons](#); (d). [Amazing Angular Unconformity \(geologyin.com\)](#); (e). [File:ASTER Richat.jpg - Wikimedia Commons](#); (f). [File:ISR-2016-Makhtesh Ramon-Geological dike.jpg - Wikimedia Commons](#).



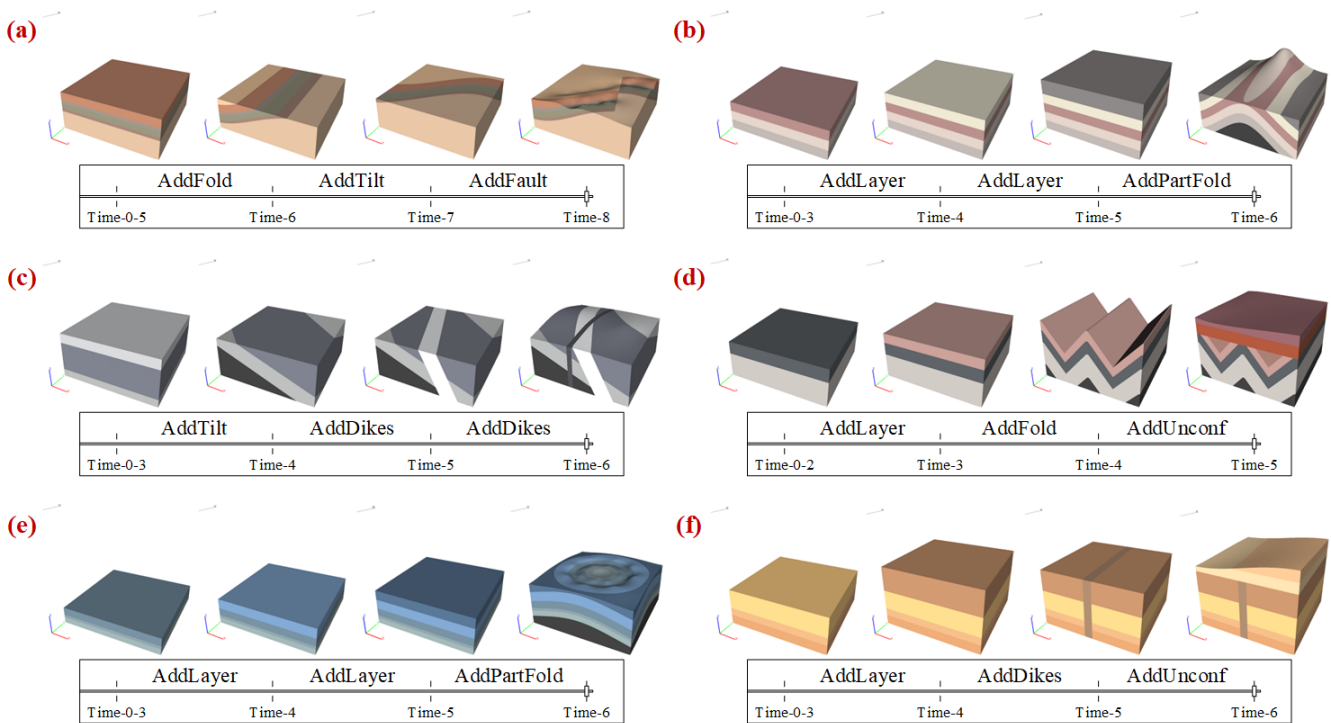
485 **Figure 21. Simulation results of typical the geologic sites.**

First, we must analyse and obtain their geological evolution to model the structural evolution of the aforementioned geological sites. The geologic sites selected in this paper all have typical structural forms; therefore, we mainly analyse the



formation process of these typical structures prior to the simulation. (a) The Piqiang Fault is on the northwest side of the Bachu Fault Zone and is connected to the Bachu Uplift in the south. Because of the uplift in the south, the stratigraphy of the area shown tends to dip to the north of the strike-slip fault (Turner et al., 2011). (b) This is a partial fold, but with erosion of relatively weak parts on both sides. (c) Based on the description and the pictures, it can be concluded that there are two successive intrusions at the site and that stratigraphic tilting occurred before the intrusion began. (d) Is a typical angular unconformity that began when the underlying strata were formed, which were then folded by crustal movement before finally being eroded and redeposited to form the overlying new strata. (e) This feature is a symmetrical and deeply eroded geodome, where a circular, symmetrical folding action occurred after the strata was deposited, which was followed by erosion to form a relatively flat geodome. (f) This feature was formed by the superposition of a dike and an unconformity; the dike occurred first, according to the image, and then the unconformity followed. The structural evolutionary processes of the above geologic features were simulated using the simulation software presented in this paper, and the results of the simulation are shown in Fig. 21.

The results show that the structural evolutionary sequence of common geologic features can be correctly simulated using the geological evolution simulation software. Through the timelines provided by the software (the timelines for the geologic features are shown in Fig. 22), the formation process and principle of typical geological structures in geological features can be dynamically observed, and the 4D reconstruction of the evolution process of geologic features can be achieved. This enables users to more clearly and intuitively understand the morphology and modes of action of local structures.



505

Figure 22. Simulation timelines for geologic features.



5 Discussion

This paper proposes a method to simplify and express various types of basic geological formations and establishes regional geological evolutionary process simulation and visualization software based on this method, which can assist geologists in explaining the evolutionary processes of geologic features. The fact that geologists find it very difficult to visualize these processes in 3D is a very common problem, therefore, these processes are still often expressed in 2D section form for geological interpretation. In practical applications, subsurface geological phenomena are by nature 3D, and it is difficult to clearly express the evolution of geological formations in 3D space using 2D sections. Our method makes it possible to represent the evolutionary geotectonic processes in a 3D environment. With two case studies, we also show that the method presented in this paper can support the rapid simulation of regional geotectonic evolutionary processes in 3D space.

Our proposed method supports the simulation of geological structures in any direction and angle within the X, Y, and Z coordinate frame and can generate vector models with smooth boundaries as compared to other methods capable of visualizing geotectonic evolutionary processes in a 3D environment. Our method summarizes and simplifies each geological structure and incorporates it into a corresponding module, which greatly facilitates the ability of the end user to simulate the structure. Additionally, our method makes it easier to extend the features and add detail to individual elements.

We use a tetrahedral grid to arrange strata and structures, and then the vector model is constructed. Therefore, it is possible to extract geological data that cannot be extracted by a raster model, such as geological boundary data. We also provide the free cutting function, which can easily obtain the geological section in any direction along the simulation model (Fig. 23). The software also preserves the interface of each geological structure so that we can generate a great quantity of simulated geological models quickly by writing scripts, and together with the geological simulation data generated, we can automatically generate a great quantity of geological models, along with their corresponding geological data, which can then be used as a training set for deep learning applications.

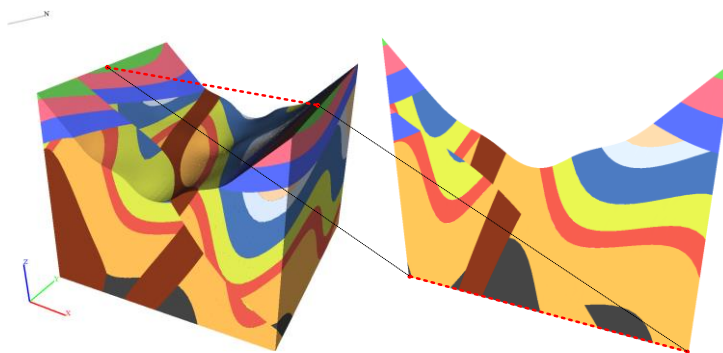


Figure 23. Free cut function.

Our method certainly has some limitations. For example, in this study we simplified individual stratum to a uniform thickness, even though the width of the stratum should be uneven and vary in thickness. Although this method provides many parameters that can add variety to the geologic elements, the final product is still far more regular that would be observed in



535 reality. Therefore, the simulation model presented here is not as precise as the model built from actual data. However, this model depicts the evolutionary process that is not reflected in the model developed from actual data. Our subsequent research may be to add more types of elements and further enrich the model to add more possibilities.

6 Conclusions

We parameterized and modularized various geological structures and developed a 4D vector modelling program, which can quickly simulate the evolution of geological structures. We then conducted experiments from two perspectives. First, we simulated the evolution of complex regional geological formations and actual well-known geological features. The results showed that software developed by this study can be used to quickly model the evolution of complex geologic structures and simulate the evolution of actual geologic features. Finally, the 4D spatial and temporal evolution of regional geologic formations is realized. This model can also dynamically present the regional geologic evolutionary process and reveal the interactions between structures over time via the timeline feature of the program. The system presented in this paper was developed around the idea of using several representative parameters to express various geological structures and encapsulate those structures within different modules. Therefore, it is more convenient to add subsequent structures and provide additional detail to a single structure.

540
545

Code availability. The source code of 4D geological structure evolution vector modelling is available at: <https://doi.org/10.5281/zenodo.7498592>

Data availability. The model data and terrain data of the case in this paper are available at: <https://doi.org/10.5281/zenodo.7498592>

550 *Video supplement.* We have provided web links to download the video recordings of our case studies. The real area case verifies the feasibility. The video supplement at: https://drive.google.com/file/d/1ngbf1E0WRhuQAby_n0EJwHJBLbAjJG7z/view?usp=sharing

Author contributions. Jiateng Guo and Zhibin Liu conceived the manuscript; Jiateng Guo provided funding support and ideas; Zhibin Liu and Xulei Wang were responsible for the research method and program development; Xulei Wang and Yunqiang Li helped to improve the modelling method and software; Lixin Wu and Shanjun Liu helped to improve the manuscript. All authors have read and agreed to the submitted version of the manuscript.

555



Competing interests. The authors declare that they have no conflict of interest.

Acknowledgements. This work was financially supported by the National Natural Science Foundation of China [grant number: 42172327] and the Fundamental Research Funds for the Central Universities [grant number: N2201022].

References

- 560 Abdullah, E. A., Abdelmaksoud, A., and Hassan, M. A.: Application of 3D Static Modelling in Reservoir Characterization: A Case Study from the Qishn Formation in Sharyoof Oil Field, Masila Basin, Yemen, *Acta Geol Sin-Engl*, 96, 348-368, <https://doi.org/10.1111/1755-6724.14766>, 2022.
- Adelu, A. O., Aderemi, A. A., Akanji, A. O., Sanuade, O. A., Kaka, S. I., Afolabi, O., Olugbemiga, S., and Oke, R.: Application of 3D static modeling for optimal reservoir characterization, *Journal of African Earth Sciences*, 152, 184-196, <https://doi.org/10.1016/j.jafrearsci.2019.02.014>, 2019.
- 565 Bagley, B., Sastry, S. P., and Whitaker, R. T.: A Marching-Tetrahedra Algorithm for Feature-Preserving Meshing of Piecewise-Smooth Implicit Surfaces, *Procedia Engineer*, 163, 162-174, <https://doi.org/10.1016/j.proeng.2016.11.042>, 2016.
- Bellahsen, N. and Fiore, P. E.: THE GROWTH OF SHEEP MOUNTAIN ANTICLINE: COMPARISON OF FIELD DATA AND NUMERICAL MODELS, 2015.
- 570 Bozzano, F., Bretschneider, A., and Martino, S.: Stress–strain history from the geological evolution of the Orvieto and Radicofani cliff slopes (Italy), *Landslides*, 5, 351-366, <https://doi.org/10.1007/s10346-008-0127-2>, 2008.
- Chen, L., Tang, D. B., Liu, X. B., Oliveira, M., and Liu, C. Q.: Evolution of the ring-like vortices and spike structure in transitional boundary layers, *Sci China Phys Mech*, 53, 514-520, <https://doi.org/10.1007/s11433-010-0129-7>, 2010.
- Cockett, R., Moran, T., and Pidlisecky, A.: Visible Geology: Creative Online Tools for Teaching, Learning, and Communicating Geologic Concepts, <https://doi.org/10.1306/13561985M1113671>, 2016.
- 575 Favre, A., Packert, M., Pauls, S. U., Jahnig, S. C., Uhl, D., Michalak, I., and Muellner-Riehl, A. N.: The role of the uplift of the Qinghai-Tibetan Plateau for the evolution of Tibetan biotas, *Biol Rev Camb Philos Soc*, 90, 236-253, <https://doi.org/10.1111/brv.12107>, 2015.
- Guo, J. T., Wang, X. L., Wang, J. M., Dai, X. W., Wu, L. X., Li, C. L., Li, F. D., Liu, S. J., and Jessell, M. W.: Three-dimensional geological modeling and spatial analysis from geotechnical borehole data using an implicit surface and marching tetrahedra algorithm, *Engineering Geology*, 284, 106047, <https://doi.org/10.1016/j.enggeo.2021.106047>, 2021.
- 580 Jessell, M., Guo, J. T., Li, Y. Q., Lindsay, M., Scalzo, R., Giraud, J., Pirot, G., Cripps, E., and Ogarko, V.: Into the Noddyverse: a massive data store of 3D geological models for machine learning and inversion applications, *Earth Syst Sci Data*, 14, 381-392, <https://doi.org/10.5194/essd-14-381-2022>, 2022.



- 585 Jessell, M. W. and Valenta, R. K.: Structural geophysics: Integrated structural and geophysical modelling, in: Structural Geology and Personal Computers, edited by: De Paor, D. G., Computer Methods in the Geosciences, Pergamon, 303-324, [https://doi.org/10.1016/S1874-561X\(96\)80027-7](https://doi.org/10.1016/S1874-561X(96)80027-7), 1996.
- Li, J. Z., Tao, X. W., Bai, B., Huang, S. P., Jiang, Q. C., Zhao, Z. Y., Chen, Y. Y., Ma, D. B., Zhang, L. P., Li, N. X., and Song, W.: Geological conditions, reservoir evolution and favorable exploration directions of marine ultra-deep oil and gas
590 in China, Petroleum Exploration and Development, 48, 60-79, [https://doi.org/10.1016/S1876-3804\(21\)60005-8](https://doi.org/10.1016/S1876-3804(21)60005-8), 2021.
- Lidal, E. M., Hauser, H., and Viola, I.: Geological storytelling: graphically exploring and communicating geological sketches, Proceedings of the International Symposium on Sketch-Based Interfaces and Modeling, 11-20, <http://dx.doi.org/10.2312/SBM/SBM12/011-020>,
- Lidal, E. M., Natali, M., Patel, D., Hauser, H., and Viola, I.: Geological storytelling, Comput Graph-Uk, 37, 445-459,
595 <https://doi.org/10.1016/j.cag.2013.01.010>, 2013.
- Matton, G. and Jébrak, M.: The “eye of Africa” (Richat dome, Mauritania): An isolated Cretaceous alkaline–hydrothermal complex, Journal of African Earth Sciences, 97, 109-124, <https://doi.org/10.1016/j.jafrearsci.2014.04.006>, 2014.
- Natali, M., Viola, I., and Patel, D.: Rapid Visualization of Geological Concepts, 2012 25th SIBGRAPI Conference on Graphics, Patterns and Images, 22-25 Aug. 2012, 150-157, <https://doi.org/10.1109/SIBGRAPI.2012.29>,
- 600 Rahbek, C., Borregaard, M. K., Antonelli, A., Colwell, R. K., Holt, B. G., Nogues-Bravo, D., Rasmussen, C. M. O., Richardson, K., Rosing, M. T., Whittaker, R. J., and Fjeldsa, J.: Building mountain biodiversity: Geological and evolutionary processes, Science, 365, 1114-1119, <https://doi.org/10.1126/science.aax0151>, 2019.
- Turner, S. A., Liu, J. G., and Cosgrove, J. W.: Structural evolution of the Piqiang Fault Zone, NW Tarim Basin, China, Journal of Asian Earth Sciences, 40, 394-402, <https://doi.org/10.1016/j.jseaes.2010.06.005>, 2011.
- 605 van Hinsbergen, D. J. J., Torsvik, T. H., Schmid, S. M., Mañenco, L. C., Maffione, M., Vissers, R. L. M., Gürer, D., and Spakman, W.: Orogenic architecture of the Mediterranean region and kinematic reconstruction of its tectonic evolution since the Triassic, Gondwana Research, 81, 79-229, <https://doi.org/10.1016/j.gr.2019.07.009>, 2020.
- Wu, L. X., Lu, J. C., Mao, W. F., Hu, J., Zhou, Z. L., Li, Z. W., Qi, Y., and Yao, R. B.: Sectional fault-inclination-change based numerical simulation of structure stress evolution on the seismogenic fault of Madoi earthquake, Chinese Journal of
610 Geophysics, 65, 3844-3857, <https://doi.org/10.6038/cjg2022P0988>, 2022.
- Geology—an Introduction. E-learning module about geology. /<http://folk.uib.no/nglhe/Emodules/GeoIntroMod.swfS>. Accessed November 2012; 2012.
- Wu, X. M., Geng, Z. C., Shi, Y. Z., Pham, N., Fomel, S., and Caumon, G.: Building realistic structure models to train convolutional neural networks for seismic structural interpretation, Geophysics, 85, Wa27-Wa39,
615 <https://doi.org/10.1190/geo2019-0375.1>, 2020.
- Zhai, M. G. and Santosh, M.: Metallogeny of the North China Craton: Link with secular changes in the evolving Earth, Gondwana Research, 24, 275-297, <https://doi.org/10.1016/j.gr.2013.02.007>, 2013.



- 620 Zhou, Q. X., Wang, S. M., Liu, J. Q., Hu, X. G., Liu, Y. X., He, Y. Q., He, X., and Wu, X. T.: Geological evolution of offshore pollution and its long-term potential impacts on marine ecosystems, *Geoscience Frontiers*, 13, 101427, <https://doi.org/10.1016/j.gsf.2022.101427>, 2022.
- Zhu, J., Zhou, X., Zhang, G., and Wang, Q.: Quaternary Depositional Framework of the Xiong’san New Area: A 3D Geological Modeling Approach Based on Vector and Grid Integration, <https://doi.org/10.3390/su14063409>, 2022.